Spatially resolved amplitude and phase characterization of femtosecond optical pulses

L. Gallmann, G. Steinmeyer, D. H. Sutter, and T. Rupp

Ultrafast Laser Physics Laboratory, Institute of Quantum Electronics, Swiss Federal Institute of Technology, ETH Hönggerberg–HPT, CH-8093 Zürich, Switzerland

C. Iaconis and I. A. Walmsley

The Institute of Optics, University of Rochester, Rochester, New York 14627

U. Keller

Ultrafast Laser Physics Laboratory, Institute of Quantum Electronics, Swiss Federal Institute of Technology, ETH Hönggerberg–HPT, CH-8093 Zürich, Switzerland

Received July 6, 2000

Ultrabroadband pulses exhibit a frequency-dependent mode size owing to the wavelength dependence of free-space diffraction. Additionally, rather complex lateral dependence of the temporal pulse shape has been reported for Kerr-lens mode-locked lasers and broadband amplifier chains and in frequency-domain pulse shapers, for example. We demonstrate an ultrashort-pulse characterization technique that reveals lateral pulse-shape variations by spatially resolved amplitude and phase measurements by use of spectral phase interferometry for direct electric-field reconstruction (SPIDER). Unlike with autocorrelation techniques, with SPIDER we can obtain spatially resolved pulse characterization even after the nonlinear process. Thus, with this method the spectral phase of the pulse can be resolved very rapidly along one lateral beam axis in a single measurement.

OCIS codes: 320.0320, 320.5550, 320.7100, 120.5050, 120.3180.

Several ultrashort-pulse measurement techniques, such as frequency-resolved optical gating[1,2] (FROG) and spectral phase interferometry for direct electric-field reconstruction[3,4] (SPIDER), have emerged that allow for full amplitude and phase characterization. So far, amplitude and phase characterization techniques have been used to perform spatially integrated measurements. Ultrabroadband pulses, however, can exhibit pronounced frequency-dependent mode sizes (FDMS's).[5] A FDMS leads to laterally changing spectral content of the beam and, consequently, to lateral dependence of the temporal pulse shape. Beams with a pronounced FDMS require a careful interpretation of spatially integrated measurements. It should be noted that nonlinear optical processes, which are also employed in most characterization methods, further enhance the frequency-dependent variations with their corresponding power law. Spatial distortions can be rather complex in broadband amplifier chains and in sub-10-fs Ti:sapphire lasers.[6]

In this Letter we discuss the influence of spatially dependent pulse parameters on pulse characterization and present a simple extension of a sub-10-fs SPIDER setup[7] that allows recording of spatial variations. The SPIDER technique is particularly attractive for this purpose because the spectral phase measurement consists of only a single acquisition of a spectrum. The noniterative reconstruction algorithm permits rapid processing of the large amount of data that results from the spatial resolution. The intrinsically fast acquisition and reconstruction were previously demonstrated in real-time variants of SPIDER with refresh rates of up to 20 Hz.[8,9] In addition, without any prior knowledge of the FDMS, autocorrelation measurements require spatial filtering before the nonlinear process, which strongly reduces signal strength. In contrast, with SPIDER we can obtain spatially resolved pulse characterization even after the nonlinear process without any prior knowledge of the FDMS. We performed spatially resolved SPIDER measurements on our sub-10-fs Ti:sapphire laser.[10]

Spatial distortions of femtosecond pulsed beams occur, for example, in pulse stretchers, amplifier chains, and frequency-domain pulse shapers. Generally these effects become more severe with a larger pulse bandwidth. Apart from these imperfections, free-space diffraction of broadband beams is an inevitable source of a spatial structure that causes a FDMS. For Gaussian beams, radius w as a function of propagation distance z is given as

$$w(z) = \sqrt{\lambda z_0/\pi}\,[1 + (z/z_0)^2]^{1/2}, \tag{1}$$

with wavelength λ and confocal parameter z_0. For beams originating from a laser cavity, confocal parameter z_0 is a constant. Therefore the mode area is proportional to the wavelength at a fixed distance z from the focus. For the nearly 1-octave-bandwidth spectra of sources in the 5-fs regime,[11] this effect can lead to spectral variations of the mode area of more than 50%.

For Kerr-lens mode-locked (KLM) lasers, complex FDMS effects have been reported.[5] Inside the gain medium of such a laser, the time-dependent Kerr lens translates the temporal intensity profile of the pulse into an accompanying spatial structure and vice versa. Thus, in such a laser the FDMS is pulse-shape dependent. Figure 1 shows measurements of the FDMS for sub-10-fs pulses from a KLM Ti:sapphire laser.[10] The mode areas have been measured with a beam profilometer and 10-nm-wide interference filters. The

0146-9592/01/020096-03$15.00/0

variation of spectral power density and mode area with wavelength reflects the dispersion oscillations[11] of the double-chirped mirrors used inside the cavity. Small adjustments of intracavity dispersion alter the temporal pulse shape in the Kerr medium, resulting in significant variations of the FDMS.

In autocorrelation or cross-correlation techniques using second-harmonic generation (SHG), such as SHG-FROG, each frequency component of a pulse is mixed with each frequency component of a gating pulse in a convolutionlike manner [Fig. 2(a)]. Ideally all these mixing processes occur with equal efficiency. However, even with perfect phase-matching conditions, the FDMS produces frequency-dependent conversion efficiency. In the simple case of pure SHG of quasi-monochromatic slices of the spectrum, for example, a 41% increase in mode area (Fig. 1) already reduces the second-harmonic signal by a factor of 2. Such efficiency variations can result in erroneous pulse characterization. Previously, the effect of the FDMS of an ideal Gaussian beam [Eq. (1)] was taken into account in SHG-FROG measurements.[12] In principle, any given FDMS can be accounted for in the reconstruction algorithm. However, this becomes increasingly difficult as the complexity of the mode structure increases. This is especially true if the mode structure changes significantly with minor adjustments of the laser, as is the case for the structures shown in Fig. 1.

The SPIDER technique uses sum-frequency generation (SFG) of two broadband input pulses delayed with respect to each other and two quasi-cw slices of a strongly linearly chirped pulse. In the spectral domain, each of these SFG processes corresponds to a convolution of a broadband spectrum with delta-function-like spectrum [Fig. 2(b)]. As a result, the input beam gets shifted in frequency space by the constant frequency and multiplied by the spatial mode pattern of that cw slice. The different frequencies of the two cw slices generate a spectral shear between the two broadband input spectra. A FDMS of the strongly chirped pulse does not cause a frequency-dependent efficiency as the same cw slice is mixed with each frequency component of the broadband input pulse. The SPIDER signal, which consists of the spectral interference of the two spectrally sheared broadband pulses, is affected only in its spatial intensity pattern, fringe contrast, and an undetermined phase constant but not in spectral fringe spacing. Because SPIDER uses only spectral fringe spacing for spectral phase reconstruction, spatially resolved SPIDER works correctly even in the presence of significant FDMS effects. Note that this implementation of SPIDER, like all self-referenced phase-measurement techniques demonstrated to date, cannot extract the linear phase term. Thus this method is not suitable for the characterization of phase-front distortions.

We implemented the spatial resolution in our setup by imaging the SPIDER signal beam and the fundamental beam from the SFG crystal on the entrance slit of a 0.3-m imaging spectrograph equipped with a 600-groove/mm grating and a two-dimensional 1024 by 128 pixel CCD camera. The SPIDER signal and the fundamental beam were measured independently. Simultaneous acquisition of both signals can be achieved by the method described in Ref. 13. The entrance slit provides the spatial resolution along one axis, while the vertical CCD dimension resolves the beam along the other axis. With the slit and the CCD we obtain an absolute spatial resolution of roughly 80 μm in each direction. The number of spatial sample points across the beam diameter can be adjusted by the choice of the magnification of the imaging optics. With this setup the spatially resolved spectral phase along one lateral beam axis is measured in a single acquisition. For access to off-axis points, the beam can be either translated sideways or rotated around its axis. Beam rotation can be achieved with a Dove prism or by out-of-plane reflection in an equivalent arrangement of mirrors.

Figure 3 shows the fundamental spectrum of our sub-10-fs Ti:sapphire laser[10] measured at three spatial positions relatively close to the beam center. With increasing distance from the center the spectra shift to longer wavelengths, which agrees favorably with the trend expected from Eq. (1). For different operating conditions of the laser, however, the KLM effect may even reverse the tendency expected from free-space diffraction. Under typical operating conditions of our laser, we find the time-dependent Kerr lens to be the dominant contribution to the FDMS (see Fig. 1). In a similar measurement, shown in Fig. 4, we observe

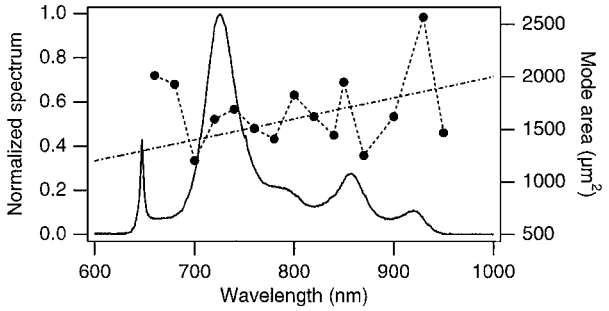

Fig. 1. Wavelength-dependent mode area of a sub-10-fs KLM Ti:sapphire laser. The spectral variation of (solid curve) the power density and (dashed curve and filled circles) the mode area reflect the dispersion oscillations of the double-chirped mirrors used inside the cavity. The dashed–dotted line shows the qualitative behavior expected from Eq. (1) (up to a scaling factor).

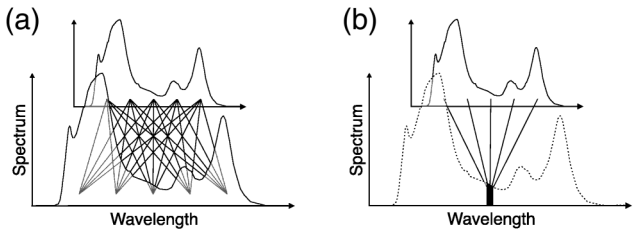

Fig. 2. Schematic picture of the mixing processes occurring in (a) broadband SHG and (b) SFG of a broadband pulse with a quasi-cw spectral slice. In SHG many different input wavelengths with differing spatial patterns are contributing to the signal at a given wavelength, whereas in SFG each individual spectral component of the signal is generated by a single mixing process.

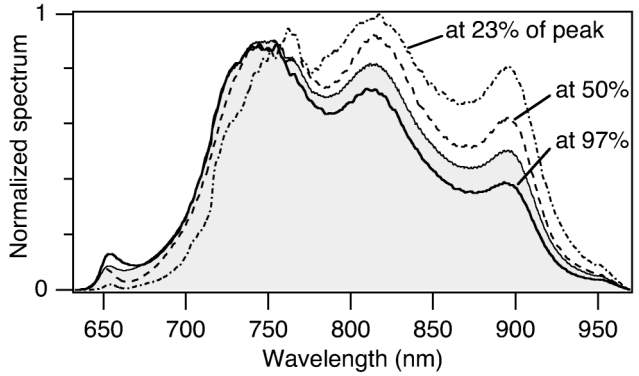

Fig. 3. Three spectra measured at different lateral positions inside the beam. For comparison the spatially integrated spectrum is also shown (shaded area).

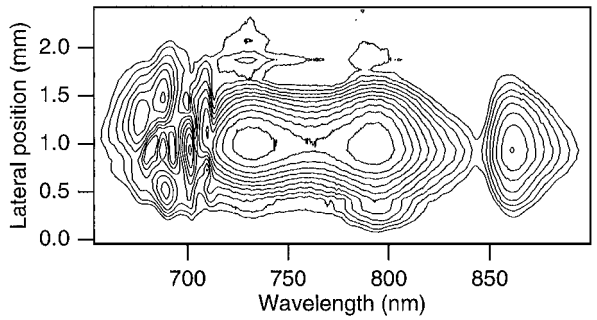

Fig. 4. Contour plot of the spatially resolved pulse spectrum. The contours are evenly spaced on a logarithmic scale and start at 0.7% of the maximum value. Note the complicated structure on the short-wavelength side.

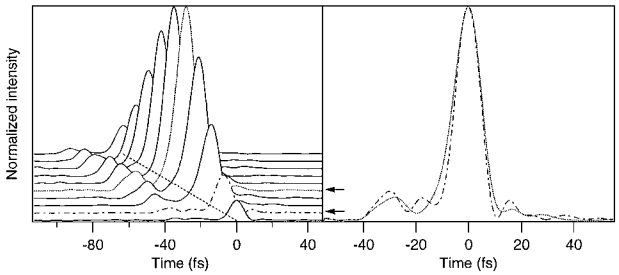

Fig. 5. Left, laterally varying temporal pulse shapes normalized to the spectrally integrated beam intensity. Right, to facilitate a direct comparison, two pulses (dotted and dashed–dotted curves) are also shown normalized to the same peak intensity. The differences are most pronounced in the temporal wings of the pulses. Nevertheless, the FWHM of the two pulses shown already differs by more than 10%.

a highly irregular structure in the short-wavelength part of the spectrum. We attribute this complicated pattern to diffraction effects that are due to slight clipping at one of the prisms, a situation that might go unnoticed in the absence of spatial resolution.

The combination of the spatially resolved spectrum and the spectral phase measurement gives one access to the full lateral dependence of the pulse shape (Fig. 5). The situation shown in Figs. 4 and 5 corresponds to a spatially averaged transform-limited pulse of 9.2-fs duration, slightly chirped to an averaged duration of 11.6 fs. A clear trend is observed even for the relatively insensitive FWHM duration. On center, the pulse has a duration of 12.3 fs, in contrast to an 11-fs duration in the wings. Note that these variations result in systematically erroneous spatially integrated measurements, with errors depending on the specific technique and the power law of the nonlinear process.

In this Letter we have demonstrated how to resolve lateral variations of the spectral and temporal pulse shape in the beam profile of a KLM Ti:sapphire laser. With the recently demonstrated high immunity of the SPIDER technique to experimental noise, an accurate pulse characterization is possible even in the low-intensity spatial or spectral wings of a beam.[14] The accuracy of the method can be further improved by suitable adaptation of the integration times to the local intensity. Spatially resolved amplitude and phase characterization should permit quantitative analysis of spatial distortions and propagation effects of femtosecond pulses. Additionally, this tool should simplify the interpretation of experimental results obtained with spatially structured beams.

This work was supported by the Swiss National Science Foundation (L. Gallmann, G. Steinmeyer, D. H. Sutter, T. Rupp, and U. Keller) and by the U.S. National Science Foundation (C. Iaconis and I. A. Walmsley). L. Gallmann's e-mail address is gallmann@iqe.phys.ethz.ch.

References

1. D. J. Kane and R. Trebino, IEEE J. Quantum Electron. **29,** 571 (1993).
2. R. Trebino, K. W. DeLong, D. N. Fittinghoff, J. Sweetser, M. A. Krumbügel, and B. Richman, Rev. Sci. Instrum. **68,** 1 (1997).
3. C. Iaconis and I. A. Walmsley, Opt. Lett. **23,** 792 (1998).
4. C. Iaconis and I. A. Walmsley, IEEE J. Quantum Electron. **35,** 501 (1999).
5. S. T. Cundiff, W. H. Knox, E. P. Ippen, and H. A. Haus, Opt. Lett. **21,** 662 (1996).
6. L. Gallmann, D. H. Sutter, N. Matuschek, G. Steinmeyer, and U. Keller, Appl. Phys. B **70,** 67 (2000).
7. L. Gallmann, D. H. Sutter, N. Matuschek, G. Steinmeyer, U. Keller, C. Iaconis, and I. A. Walmsley, Opt. Lett. **24,** 1314 (1999).
8. T. M. Shuman, M. E. Anderson, J. Bromage, C. Iaconis, L. Waxer, and I. A. Walmsley, Opt. Express **5,** 134 (1999), http://epubs.osa.org/opticsexpress.
9. C. Dorrer, B. de Beauvoir, C. Le Blanc, S. Ranc, J. P. Rousseau, J. P. Chambaret, and F. Salin, Opt. Lett. **24,** 1644 (1999).
10. D. H. Sutter, G. Steinmeyer, L. Gallmann, N. Matuschek, F. Morier-Genoud, U. Keller, V. Scheuer, G. Angelow, and T. Tschudi, Opt. Lett. **24,** 631 (1999).
11. G. Steinmeyer, D. H. Sutter, L. Gallmann, N. Matuschek, and U. Keller, Science **286,** 1507 (1999).
12. A. Baltuska, M. S. Pshenichnikov, and D. A. Wiersma, IEEE J. Quantum Electron. **35,** 459 (1999).
13. C. Dorrer, Opt. Lett. **24,** 1532 (1999).
14. M. E. Anderson, L. E. E. de Araujo, E. M. Kosik, and I. A. Walmsley, Appl. Phys. B **70,** 85 (2000).